

Industrial Chemistry & Materials

Accepted Manuscript

This article can be cited before page numbers have been issued, to do this please use: B. Yu, M. Yang, Y. Qiao, Y. Wang, Y. Xu, X. Bie, Q. Li, Y. Zhang, S. Sun and H. Zhou, *Ind. Chem. Mater.*, 2025, DOI: 10.1039/D5IM00087D.



This is an Accepted Manuscript, which has been through the Royal Society of Chemistry peer review process and has been accepted for publication.

Accepted Manuscripts are published online shortly after acceptance, before technical editing, formatting and proof reading. Using this free service, authors can make their results available to the community, in citable form, before we publish the edited article. We will replace this Accepted Manuscript with the edited and formatted Advance Article as soon as it is available.

You can find more information about Accepted Manuscripts in the [Information for Authors](#).

Please note that technical editing may introduce minor changes to the text and/or graphics, which may alter content. The journal's standard [Terms & Conditions](#) and the [Ethical guidelines](#) still apply. In no event shall the Royal Society of Chemistry be held responsible for any errors or omissions in this Accepted Manuscript or any consequences arising from the use of any information it contains.

ARTICLE

Integrated SO₂/NO₂-containing CO₂ capture and methane dry reforming over Ni-Ca dual functional material: A mechanistic study

Received 00th January 20xx,
Accepted 00th January 20xx

DOI: 10.1039/x0xx00000x

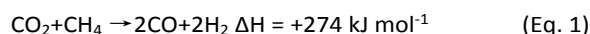
Bocheng Yu,^a Muqing Yang,^a Yijian Qiao,^a Yaozu Wang,^a Yongqing Xu,^a Xuan Bie,^a Qinghai Li,^a Yanguo Zhang,^a Shuzhuang Sun^{*b} and Hui Zhou^{*ac}

Integrated carbon capture and utilization (ICCU) has emerged as a promising strategy toward carbon neutrality. However, most existing studies rely on simulated flue gas compositions, neglecting the impact of common impurities such as sulfur oxides (SO_x) and nitrogen oxides (NO_x), thereby limiting the practical industrial applicability of ICCU technologies. Herein, we systematically investigate the effects of SO₂ and NO₂ at various concentrations on the adsorption-catalysis performance based on a representative Ni-Ca dual functional material (DFM) in ICCU-dry reforming of methane (ICCU-DRM) process. Exposure to 100 ppm SO₂ showed negligible influence on catalytic activity but markedly inhibited carbon deposition. Further increasing the SO₂ concentration to 500 ppm led to complete deactivation of the DFM. NO₂ exhibited a similar concentration-dependent trend to SO₂, albeit with a comparatively lower impact. Mechanistic analysis revealed that both SO₂ and NO₂ promote the formation of a coating layer of calcium-containing compounds on the surface of Ni nanoparticles, accounting for the part or total deactivation. These findings offer critical insights into the industrial applications of ICCU systems under realistic flue gas conditions.

Keywords: Integrated carbon capture and utilization; SO_x and NO_x; Deactivation; Phase transition; DRM.

1. Introduction

Excessive anthropogenic CO₂ emissions are causing severe global warming, leading to the frequent occurrence of extreme weather.^{1,2} Carbon capture, utilization and storage (CCUS) are believed as one of the most promising ways to achieve net zero by this mid-century as an industrial-level technology.^{3–5} Compared to carbon capture and storage (CCS), carbon capture and utilization (CCU) can convert the captured CO₂ into high-value chemical products (CO, CH₄, CH₃OH, etc.), which shows a better economy with the avoidance of carbon leaks. Among most of the C1 production reactions (reverse water gas shift, methanation, etc.), dry reforming of methane (DRM, Eq. 1) can simultaneously convert two main greenhouse gases CH₄ and CO₂ into syngas, which serves as a feedstock for other important chemical reactions like methanol production and Fischer-Tropsch synthesis.^{6,7} However, high CO₂ storage and transportation costs and massive energy consumption on temperature and pressure swing operations severely restrain the wide deployment of CCU technologies.^{8,9}



Recently, by combining the CO₂ capture and chemical utilization into one reactor, integrated carbon capture and utilization (ICCU) has gained increasing interest from researchers and engineers.^{10–14} To achieve these two processes in one reactor, dual function materials (DFMs), consisting of adsorptive component for carbon capture and catalytic component for carbon

^a Key Laboratory for Thermal Science and Power Engineering of Ministry of Education, Beijing Key Laboratory of CO₂ Utilization and Reduction Technology, Department of Energy and Power Engineering, Tsinghua University, Beijing 100084, P.R. China.

^b School of Chemical Engineering, Zhengzhou University, Zhengzhou 450001, P.R. China.

^c Shanxi Research Institute for Clean Energy, Tsinghua University, Taiyuan, Shanxi 030000, P.R. China

^d * Corresponding authors. Emails: ssun@zzu.edu.cn; hui Zhou@tsinghua.edu.cn.



conversion, are crucial to achieve high performance ICCU process.^{15–18} Since DRM is a strongly endothermic reaction and needs high temperature condition (600–900°C), Ca-based sorbents are the most promising candidates for carbon capture.^{19,20} However, Ca-based sorbents severely suffer from sintering, leading to a sharp decreased CO₂ capacity after cycles.^{21,22} Thus, promoters including MgO, Al₂O₃ and ZrO₂ are commonly introduced into the DFMs to enhance the CaO stability by acting as the physical barrier.^{23–25} Ni as an earth-abundant metal, showing excellent catalytic activity to methane activation, has become one of the most impressive choices for the catalytic components.^{26–28}

Previous studies focused on the outperformed DFM design and adsorptive-catalytic mechanism investigation via ideal flue gas (a mixture of CO₂ and N₂), while few studies investigate the influence of impurity components in the realistic flue gas. SO_x and NO_x, as two of the most important pollutions in flue gas, have been proven to significantly influence the capture and conversion performance.^{29–31} Previous studies reported that SO₂ and NO₂ could poison the CO₂ hydrogenation catalysts, primarily attributed to the strong chemisorption of intermediate species on active metal sites or generation of stable metal sulfides which irreversibly block active sites.^{32,33} Also, as an alkaline sorbent, CaO can adsorb acidic SO₂ and NO₂, affecting its adsorptive performance.^{34,35} Notably, as for the ICCU-DRM process, the reaction atmosphere frequently switches between oxidizing atmosphere (CO₂/N₂) and reductive atmosphere (CH₄/N₂), which brings new understandings compared to independent capture or conversion scenarios.

Herein, we investigated the influence of SO₂ and NO₂ on typical Ni-Ca DFMs. Ni5Al15Ca DFM as a representative DFM for ICCU-DRM was synthesized by the sol-gel methods, in which Ni provides high catalytic activity, CaO captures CO₂ in flue gas and Al₂O₃ acts as stabilizer. Series tests under different SO₂ and NO₂ concentrations were performed to uncover the influence of the pollution in flue gas. Low concentration of SO₂ (100 ppm) containing in flue gas showed negligible influence on catalytic activity but markedly reduced H₂:CO ratio. Further increasing the SO₂ concentration to 500 ppm resulted in complete deactivation of the DFM. NO₂ showed a similar phenomenon to SO₂ with a comparatively lower impact. Systematic characteristics were performed and revealed that the formation of a coating layer on the surface of Ni nanoparticles induced by SO₂ and NO₂, accounting for the part or total deactivation. This study aims to offer critical insights into the industrial applications of ICCU systems under realistic flue gas conditions.

2. Results and discussion

2.1 Performance evaluation of SO₂ and NO₂ influence

The impact of SO₂ and NO₂ in flue gas on the performance of ICCU-DRM was evaluated through a series of tests under varying SO₂ and NO₂ concentrations (100, 200, and 500 ppm). Without SO₂ or NO₂ in flue gas, the performance of the Ni5Al15Ca DFM was first assessed in the absence of SO₂ and NO₂. The real-time concentrations of CO₂, CO, H₂, and CH₄ during the first and second cycles are shown in Fig. 1. During the CO₂ capture stage, CO₂ was adsorbed by CaO, accompanied by CO formation attributed to the reverse Boudouard reaction (CO₂+C→2CO) from the second cycle. The elevated CO amount indicate the severe carbon deposition during the previous dry reforming stage. In the subsequent dry reforming stage, CH₄ reacted with the captured CO₂ to produce CO and H₂. Simultaneously, CH₄ could decompose into carbon and H₂ as a common side reaction. Notably, although CO was no longer detected at the final of dry reforming stage, H₂ remained generated, highlighting the strong CH₄ decomposition activity of Ni sites.

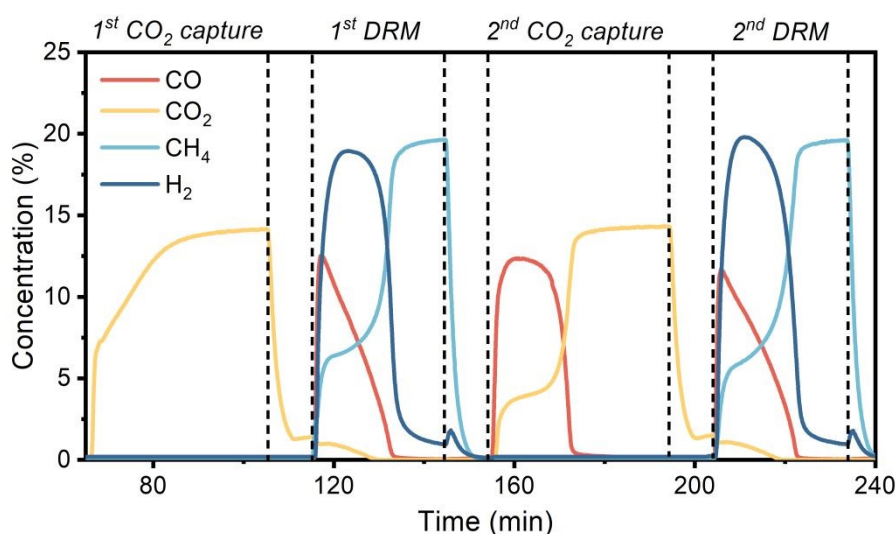


Fig. 1 Real-time gas concentrations of ICCU-DRM for the first and second cycle.

The cyclic performance of the Ni5Al15Ca DFM was systematically evaluated, as illustrated in Fig. 2. CO₂ conversion as a primary indicator of catalytic efficiency reached 81.3% in the first cycle and exhibited only a slight decline to 76.3% after 10 cycles (Fig. 2a). Result confirms the high activity and stability of the Ni active sites to dry reforming process. Despite the CO₂ conversion, the H₂:CO ratio was notably higher than the ideal stoichiometric value of 1, reaching 2.39 in the first cycle (Fig. 2b). This deviation suggests the occurrence of CH₄ decomposition as a side reaction, which contributes to excess hydrogen production and promotes carbon deposition on the catalyst surface. The elevated carbon accumulation was further evidenced by the CO yield during the carbonation stage (Fig. 2d). Notably, the CO₂ capacity of Ni5Al15Ca remained relatively stable over the 10 cycles, only decreasing from 10.9 to 9.5 mmol g⁻¹ (Fig. 2c). Such stability is attributed to the presence of Al₂O₃, which can act as a physical barrier during cycles.

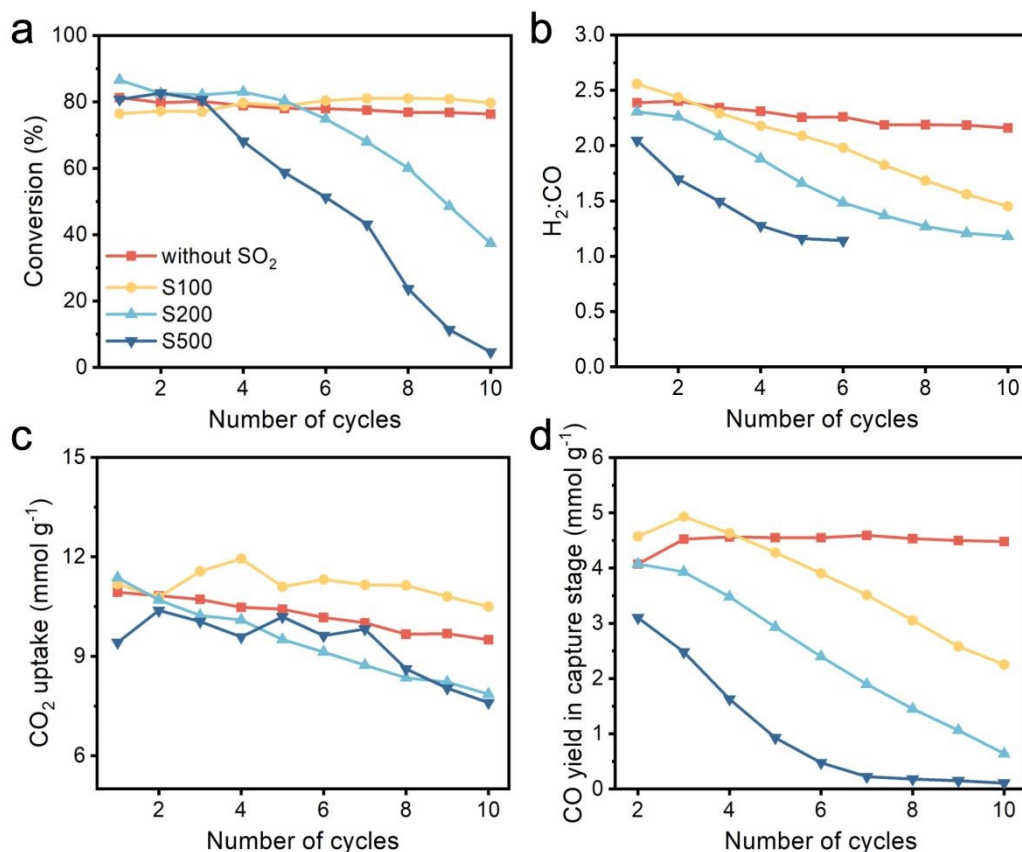


Fig. 2 Cyclic performance of ICCU-DRM under SO₂-containing flue gas.

(a) CO₂ conversion, (b) H₂:CO ratio, (c) CO₂ uptake and (d) CO yield in capture stage. S100 refers to the cycled DFM with 100 ppm SO₂ in flue gas.

The influence of varying SO₂ concentrations (100, 200, and 500 ppm) on the performance of the Ni5Al15Ca DFM was investigated. As shown in Fig. 2a, under 100 ppm SO₂ condition, the DFM reached CO₂ conversion of 79.4% in the 10th cycles, even slightly higher than the SO₂-free DFM. However, as for 200 ppm SO₂, a significant decline in CO₂ conversion was observed over cycles, with CO₂ conversion dropping to just 37.4% for the 10th cycle. Further increasing the SO₂ concentration to 500 ppm resulted in severe deactivation, with CO and H₂ becoming undetectable in the 10th cycle. Results demonstrate that low SO₂ concentration show negligible impact on the CO₂ conversion performance, while higher concentrations lead to significant DFM deactivation for ICCU-DRM.

The H₂:CO ratio as another key performance indicator was also examined, as presented in Fig. 2b. Interestingly, under 100 ppm SO₂, the H₂:CO ratio gradually decreased over cycles and approached the ideal stoichiometric value of 1, and a similar but more significant trend can be observed at 200 ppm SO₂. Results suggest that SO₂ in flue gas can suppress the CH₄ decomposition side reaction, thereby mitigating carbon deposition. Decreasing carbon deposit could further be supported by the decreased CO yield during the subsequent carbonation stage (Fig. 2d). Since both CO and H₂ production diminished to near-zero levels after the 6th cycle under 500 ppm SO₂, the H₂:CO ratio was irrelevant in the final 4 cycles. Notably, the absence of CO during the carbonation stage under 500 ppm SO₂ condition also suggested that no carbon deposition occurred.



Collectively, these findings indicate that SO₂ can reduce carbon deposition and improve product selectivity for dry reforming process.

DOI: 10.1039/D5IM00087D

The observed differences in CO₂ conversion and H₂:CO ratio between SO₂-containing and SO₂-free conditions can be attributed to different reaction kinetics. Thus, the real-time gas concentrations for the 1st and 10th cycles are presented in Fig. 3. For the Ni5Al15Ca DFM under SO₂-free condition, negligible differences were observed between the 1st and 10th cycles, suggesting that the Ni active sites remained catalytically stable for both methane dry reforming and methane decomposition. However, after introducing low concentrations of SO₂ to DFM, a rapid catalytic activity loss was observed, evidenced by the slower formation of both CO and H₂. SO₂ exhibited a more pronounced inhibitory effect on CH₄ decomposition than on the dry reforming reaction, resulting in relatively unchanged CO₂ conversion but a significantly decreased H₂:CO ratio. This shift indicates a suppression of the side reaction responsible for excess methane consumption and carbon deposition. At higher SO₂ concentrations, however, the CO₂ conversion itself became adversely affected, resulting in nearly complete deactivation.

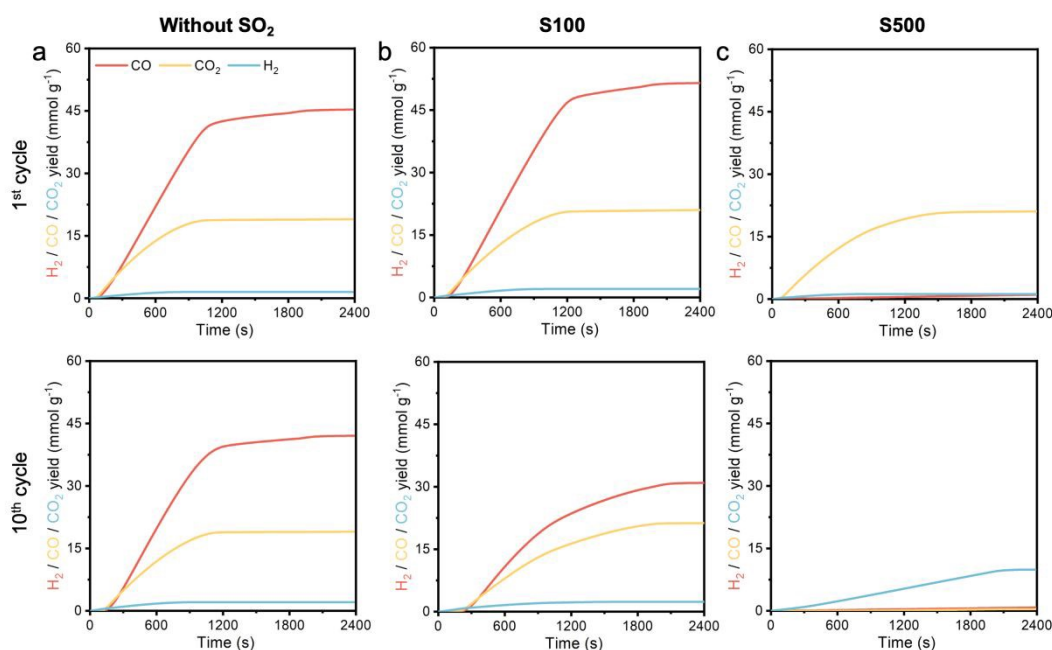


Fig. 3 Real-time gas concentration with SO₂-containing flue gas of ICCU-DRM for the 1st and 10th cycles.

(a) without SO₂ or NO₂ in flue gas, (b) 100 ppm SO₂-containing flue gas, and (c) 500 ppm SO₂-containing flue gas.

Furthermore, the effect of SO₂ on the cyclic stability of CO₂ capture by the Ni5Al15Ca DFM was assessed, as shown in Fig. 2c. Under 100 ppm SO₂, the initial CO₂ uptake was comparable to the SO₂-free condition. Notably, Ni5Al15Ca even exhibited an improved capacity retention under such condition, with only 6.1% decrease after 10 cycles, compared to 13.6% decrease observed in the DFM without SO₂ or NO₂. Enhanced stability could be attributed to the formation of thermally stable species such as CaS and CaSO₄ (vide infra), which could act as physical barriers to suppress the CaO sintering. However, increasing SO₂ concentrations led to declined CO₂ uptake with cycling. Such deactivation was likely due to the continuous formation of CaS and CaSO₄, consuming active CaO components and thereby reducing the theoretical CO₂ capacity of the DFM. In short, while limited formation of these sulfur-containing phases may enhance stability by serving as physical barriers, excessive accumulation compromises the sorbent capacity until equilibrium is reached.

The influence of NO₂ in the flue gas was further investigated, as shown in Fig. 4. Similar to SO₂, NO₂ induced a similar CO₂ conversion but a shift in the H₂:CO ratio; however, its impact was significantly less severe. Notably, the Ni5Al15Ca DFM retained considerable catalytic activity even under 500 ppm NO₂, whereas complete deactivation occurred under the same concentration of SO₂. These differences can be attributed to the relatively milder deactivation of Ni active sites by NO₂, as compared to SO₂, for both dry reforming and methane decomposition reactions (Fig. 5). In addition, NO₂ had minimal effect on CO₂ uptake capacity, likely because nitrogen species do not accumulate within the DFM (vide supra). Overall, while NO₂ exhibits a similar mode of influence to SO₂, its detrimental effects are significantly less pronounced.



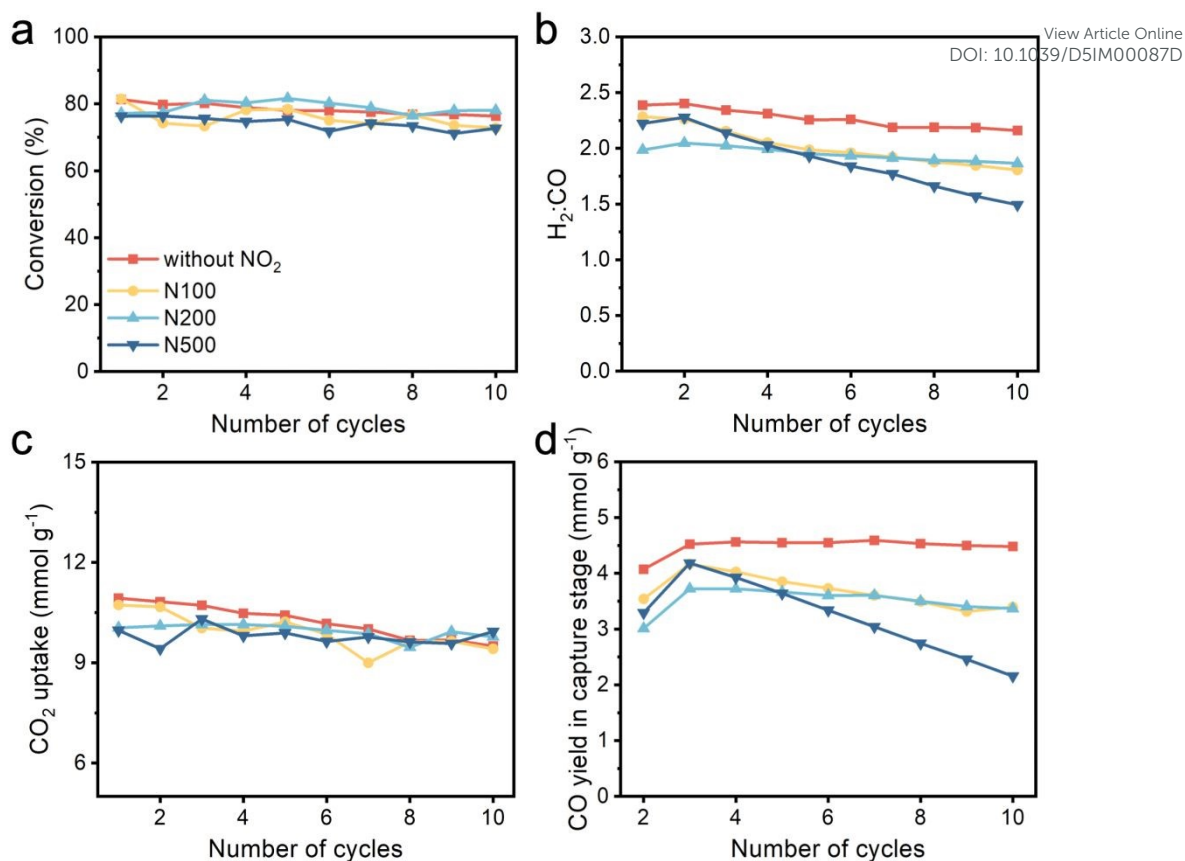


Fig. 4 Cyclic performance of ICCU-DRM under NO_2 -containing flue gas.

(a) CO_2 conversion, (b) H_2/CO ratio, (c) CO_2 uptake and (d) CO yield in capture stage. N100 refers to the cycled DFM with 100 ppm NO_2 in flue gas.

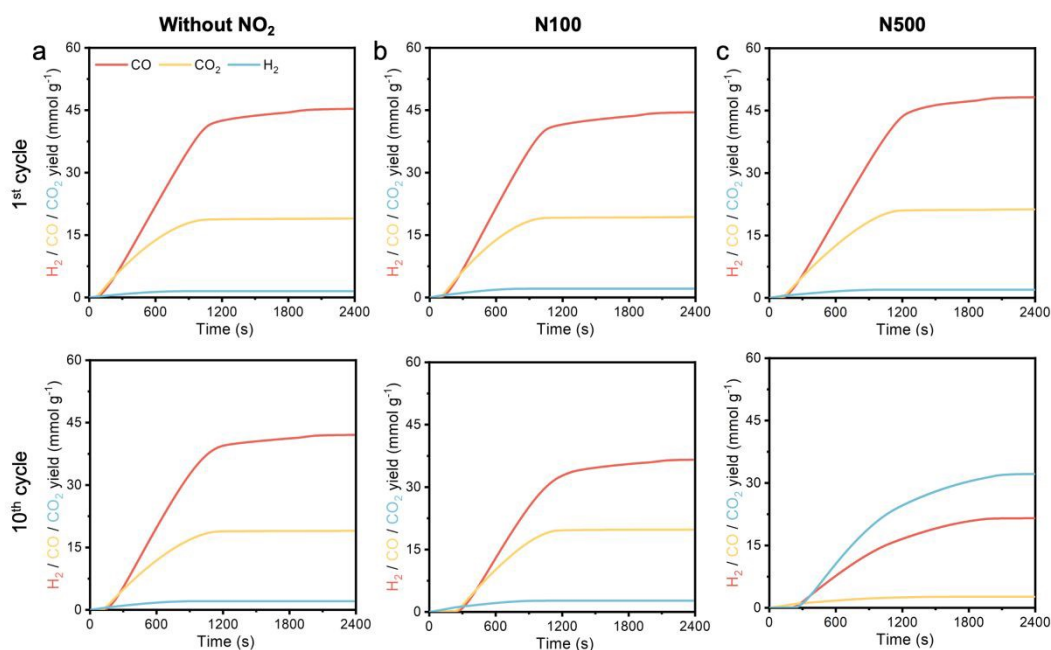


Fig. 5 Real-time gas concentration with NO_2 -containing flue gas of ICCU-DRM for the 1st and 10th cycles.

(a) without SO_2 or NO_2 in flue gas, (b) 100 ppm NO_2 -containing flue gas, and (c) 500 ppm NO_2 -containing flue gas.



2.2 Mechanism study of the SO₂ and NO₂ influences

To elucidate the performance impacts of SO₂ and NO₂, a series of systematic characterizations were conducted to reveal the underlying mechanisms. The elemental composition of the as-synthesized Ni5Al15Ca material, determined by inductively coupled plasma optical emission spectroscopy (ICP-OES), is summarized in Table 1. X-ray diffraction (XRD) (Fig. 6a) indicated that the pre-reduced Ni5Al15Ca was primarily composed of CaO (PDF# 96-900-8606) and metallic Ni (PDF# 96-151-2527), while Al existed in an amorphous phase. Scanning electron microscopy (SEM) revealed that the pre-reduced Ni5Al15Ca DFM possessed a porous morphology (Fig. 6b), and transmission electron microscope (TEM) further confirmed the dispersion of Ni nanoparticles on the blocky CaO support (Fig. 6c). N₂ physisorption measurements (Fig. 6d) showed a specific surface area of 13.4 m² g⁻¹ with an average pore diameter of 23.6 nm, indicative of a mesoporous structure of DFM. H₂ temperature-programmed reduction (H₂-TPR) analysis (Fig. 6e) demonstrated the reducibility of NiO or Ni–Al spinel species to metallic Ni under H₂, which was consistent with the XRD and TEM observations. The CO₂ uptake capacity of the pre-reduced DFM was measured to be 10.4 mmol g⁻¹ by thermal gravimetric analyzer (TGA), in good agreement with the results obtained from the fixed-bed reactor experiments (Fig. 6f).

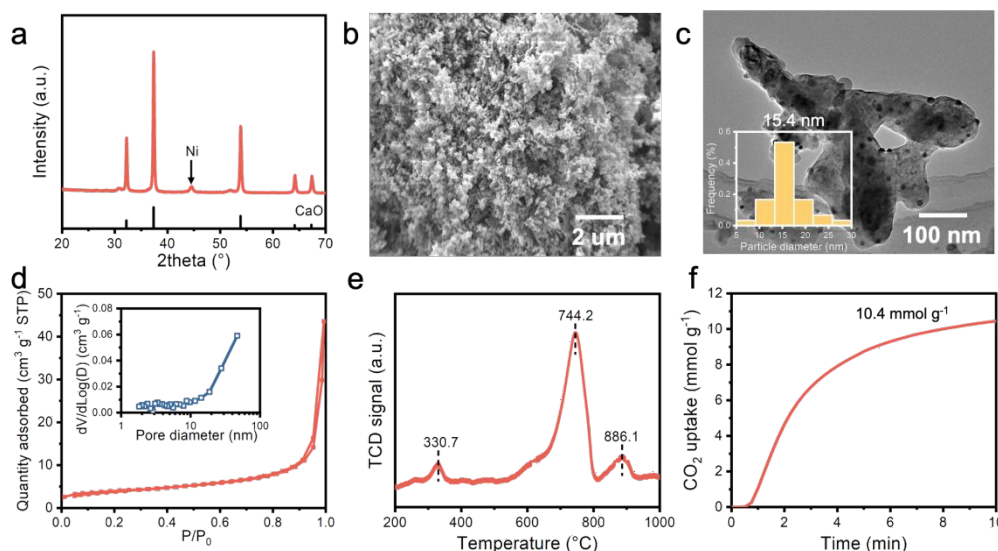


Fig. 6 Characteristics of pre-reduced Ni5Al15Ca dual functional material.

(a) XRD of pre-reduced DFM, (b) SEM of pre-reduced DFM, (c) TEM of pre-reduced DFM, (d) surface area and pore diameter distribution of the pre-reduced DFM, (e) H₂-TPR of calcined DFM and (f) TGA of pre-reduced DFM.

Table 1. Elementary analysis of pre-reduced and cycled DFM.

DFM	Ni ^a (%)	Al (%)	Ca (%)	S (%)
Pre-reduced	5.1	6.6	57.1	-
Cycled-S100	4.2	6.0	45.6	1.6
Cycled-S500	4.1	5.8	44.5	5.9

^a Mass ratio of Ni, Al, Ca and S was tested by ICP-OES

The crystal structures of cycled Ni5Al15Ca DFMs were analyzed by XRD, as shown in Fig. 7. After 10 cycles under SO₂- and NO₂-free conditions, the characteristic phases of CaO and metallic Ni remained detectable, although the significant decrease in peak intensity was attributed to the formation of amorphous carbon deposits. When cycled in flue gas containing SO₂, new diffraction peaks corresponding to CaS (PDF# 96-900-8607) appeared at both 100 ppm and 500 ppm SO₂ concentrations, whereas a minor CaSO₄ (PDF# 96-900-4097) phase was only observed at 500 ppm SO₂. The accumulation of sulfur species after 10 cycles in SO₂-containing atmospheres was further confirmed by ICP-OES. Given the relative stability of CaSO₄ and CaS under dry reforming conditions, the sulfur content reached approximately 1.6% and 5.9% for the 100 ppm and 500 ppm SO₂ cases, respectively (Table 1). However, for the samples exposed to NO₂-containing flue gas, only CaO and Ni phases were detected by XRD. Notably, higher NO₂ concentrations corresponded to increased peak intensities, consistent with the suppression of carbon deposition (vide supra). Elemental analysis showed no detectable nitrogen in the cycled DFM, indicating that nitrogen species did not accumulate during methane dry reforming.



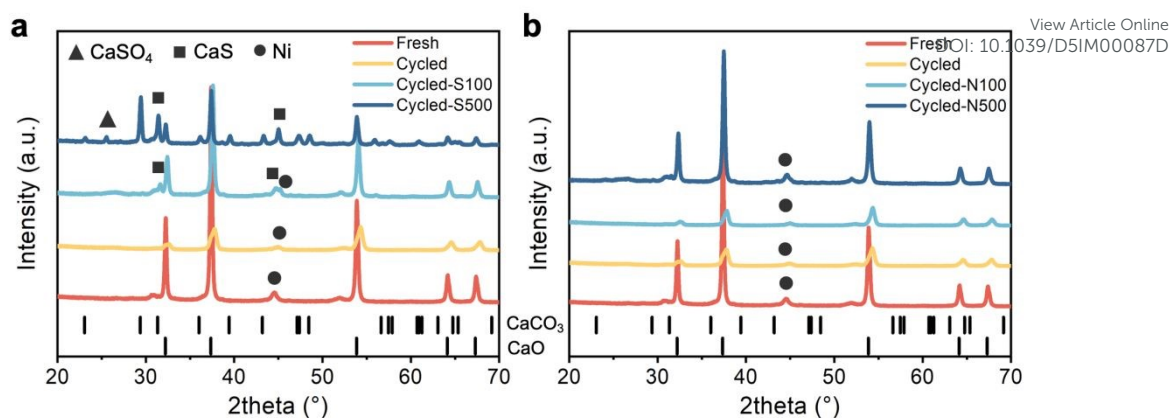


Fig. 7 XRD of pre-reduced and cycled DFMs.

(a) SO₂-containing and (b) NO₂-containing flue gas.

Given the significant impact of SO₂ on the crystal phase changing of the DFM, in situ XRD was conducted to elucidate the dynamic phase transformations during the carbonation and dry reforming stages (Fig. 8). Upon introduction of SO₂-containing flue gas into the reactor, the characteristic CaO peaks gradually diminished concurrent with the emergence of CaCO₃ peaks (PDF# 96-900-0967), confirming effective CO₂ capture. Notably, CaSO₄ was detected at the onset of the carbonation stage, reflecting the adsorption of SO₂ by the CaO sorbent. As the reaction progressed, CaS formation could be observed, likely resulting from the disproportionation of SO₂ (Eq. 2). During the conversion stage, in addition to the decomposition of CaCO₃ regenerating CaO, an increase in CaS peak intensity accompanied by a decrease in CaSO₄ peak intensity was detected. This trend is consistent with the reduction of CaSO₄ by CH₄ to form CaS (Eq. 3) ³⁶.

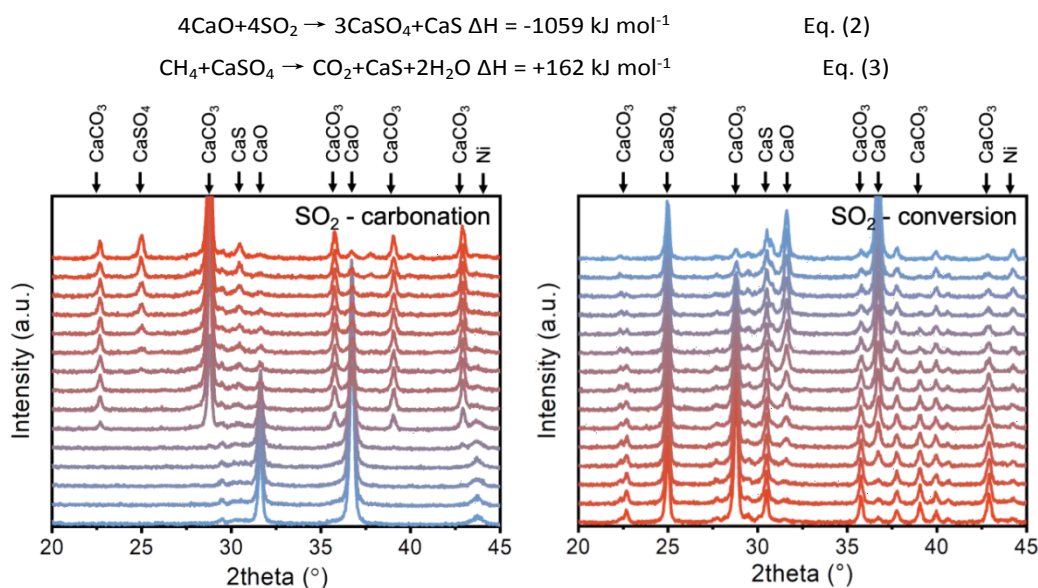


Fig. 8 In situ XRD of ICCU-DRM under SO₂-containing flue gas.

Each scan continued for 2.5 min.

The surface morphologies of the cycled DFMs are shown in Fig. 9. Severe pore collapse was observed after cycling, suggesting that the Ni5Al15Ca DFM underwent significant sintering. Notably, no discernible morphological differences could be observed between DFMs cycled in SO₂- or NO₂-containing atmospheres to without SO₂ or NO₂ condition, indicating that SO₂ and NO₂ had minimal influence on surface morphology. However, both SO₂ and NO₂ exhibited clear effects on the pore structure, as evidenced by N₂ physisorption analysis (Fig. 10 and Table 2). Compared with the pre-reduced DFM, most cycled samples, except for the DFM exposed to 500 ppm SO₂, exhibited an increase in surface area, primarily due to carbon deposition. Prior studies have shown that sintering of CaO-based DFMs typically results in a decreased pore diameter due to the collapse of macropores. In the presence of SO₂, the average pore diameter increased to 24.2 nm and 33.0 nm (at 100 ppm and 200 ppm, respectively), in contrast to the 16.8 nm observed in the SO₂-free cycled DFM. Increased pore diameter



was likely due to the formation of CaS and CaSO₄, as confirmed by XRD. Sulfur-containing species was ascribed to the increased Tammann temperatures, which function as physical barriers to effectively suppress CaO sintering. Interestingly, a similar trend could be observed in the NO₂-containing case, despite the absence of stable nitrogen-containing crystal phases. The increase in pore diameter for NO₂-treated DMF was hypothesized to result from pore generation during the decomposition of transient calcium nitrite intermediates.

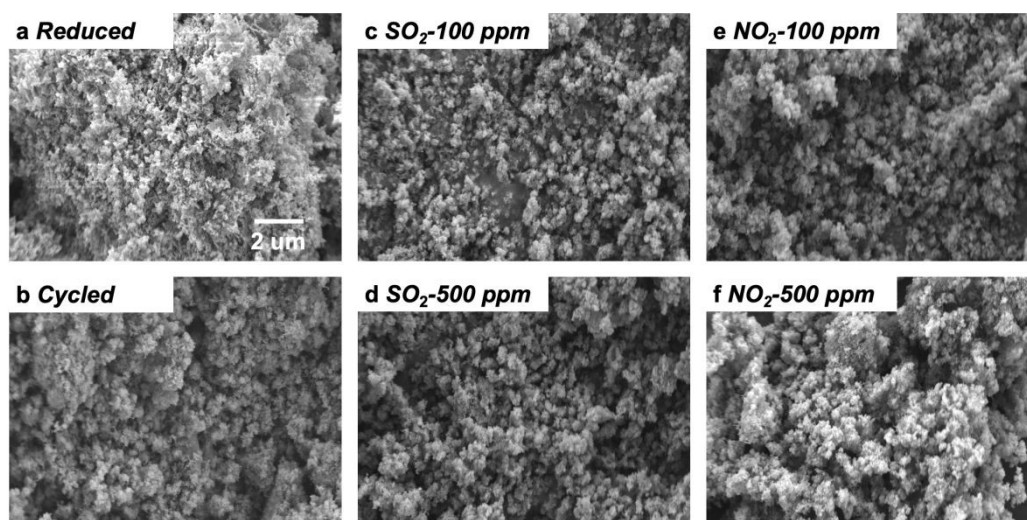


Fig. 9 SEM of pre-reduced and cycled Ni5Al15Ca DFM.

(a) Pre-reduced DFM, (b) cycled DFM without SO₂ or NO₂, (c) cycled DFM with 100 ppm SO₂-containing flue gas, (d) cycled DFM with 500 ppm SO₂-containing flue gas, (e) cycled DFM with 100 ppm NO₂-containing flue gas, and (f) cycled DFM with 500 ppm NO₂-containing flue gas.

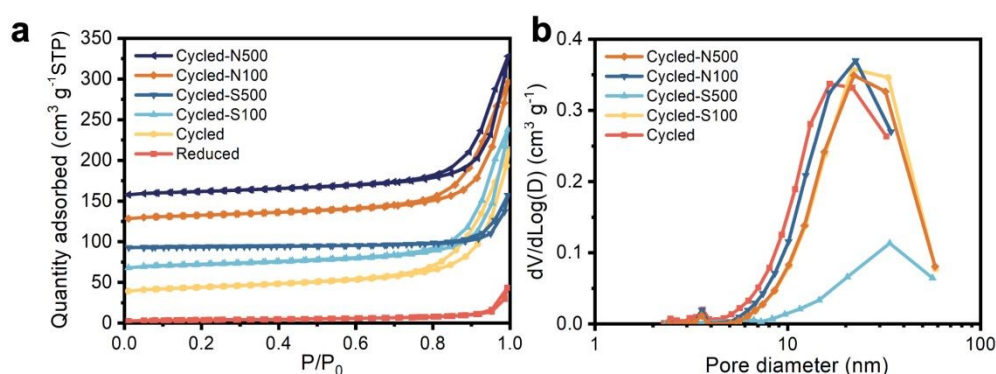


Fig. 10 N₂ physisorption of cycled DFM.

(a) BET surface and (b) pore diameter distribution.

Table 2. BET surface and averaged pore diameter of pre-reduced and cycled DFM.

DFM	BET surface (m ² g ⁻¹)	Averaged pore diameter ^a (nm)
Pre-reduced	13.4	23.6
Cycled	49.6	16.8
Cycled-S100	42.0	24.2
Cycled-S500	13.0	33.0
Cycled-N100	44.5	18.9
Cycled-N500	41.8	24.2

^aThe pore diameter was calculated by BJH desorption branch (4V/A).



The Ni nanoparticles and elemental distribution were further examined by TEM equipped with energy-dispersive X-ray analysis (EDX), as shown in Fig. 11. Pre-reduced and cycled DFM exhibited similar Ni nanoparticle size, indicated that sintering played a minor role in deactivation of Ni active sites. After 10 cycles without SO₂ or NO₂, carbon nanotubes (CNTs) were observed, originating from carbon deposition during CH₄ decomposition. Under 100 ppm SO₂, the morphology of Ni nanoparticles remained unchanged, indicating that low-concentration SO₂ exhibited minimal influence on the nano structure. However, at elevated SO₂ concentrations (500 ppm), CNTs were no longer observed, which was consistent with the reduced carbon deposition observed in fixed-bed reactor tests. Line-scan EDX analysis revealed a strong spatial correlation between sulfur and nickel signals (Fig. 11c), even though no NiS phases were detected by XRD. Close-up lattice-resolved imaging further confirmed the presence of NiS by identifying lattice fringes with a spacing of 0.322 nm, corresponding to the (111) crystal plane of NiS. These results suggest that sulfur, likely in the form of CaS or NiS, coated the surface of Ni nanoparticles, leading to blockage of active sites and consequent catalytic deactivation. In the case of NO₂-containing flue gas, similar nanoparticle morphology was observed, while N element was undetectable in the EDX, in agreement with bulk elemental analysis. Although NO₂ did not leave a residual nitrogen species on the DFM after cycling, TEM images (Fig. 11e) revealed a distinct coating layer of CaO. This could be attributed to the acidic nature of NO₂, which likely promote surface restructuring of the alkaline CaO, resulting in the formation of a coating layer.

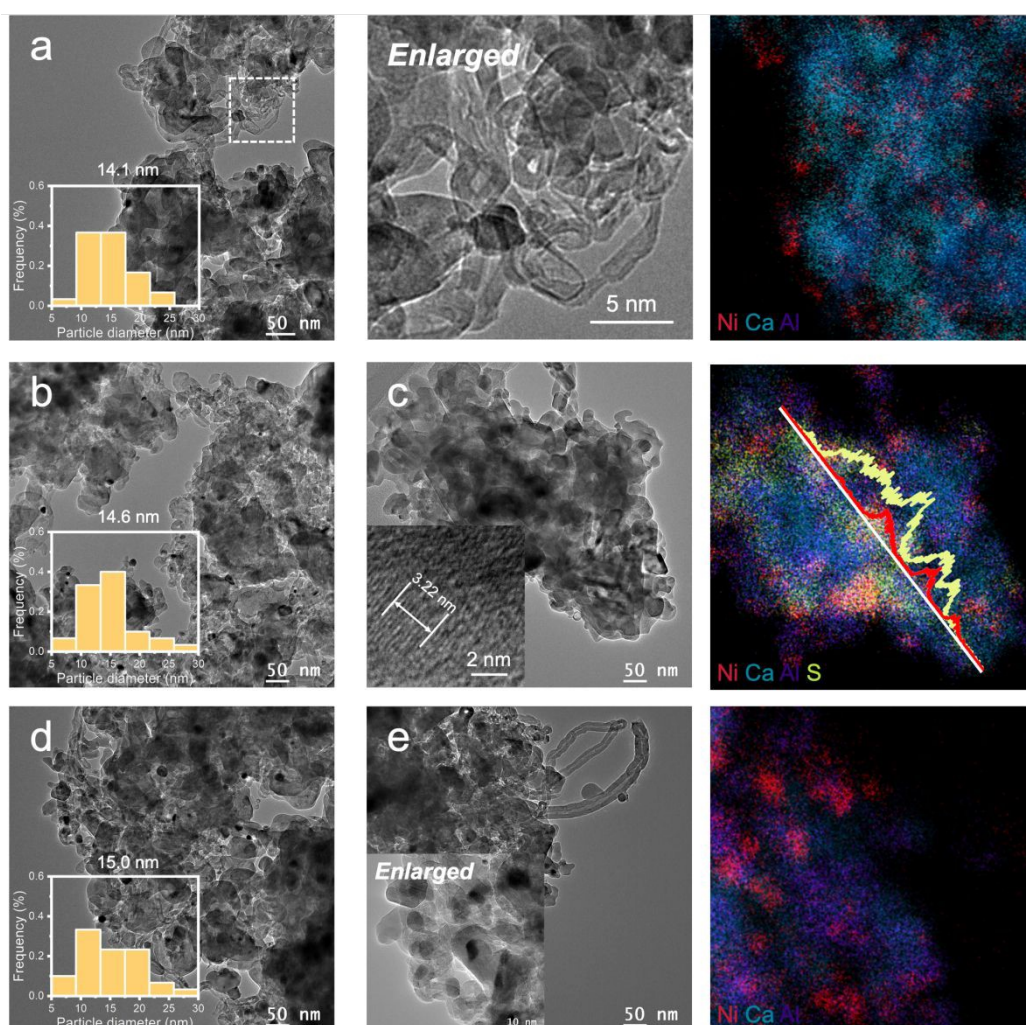


Fig. 11 TEM of cycled DFM.

(a) Cycled DFM with enlarged CNTs and EDX; (b) cycled DFM under 100 ppm SO₂-containing flue gas; (c) cycled DFM under 500 ppm SO₂-containing flue gas and EDX; (d) cycled DFM under 100 ppm NO₂-containing flue gas; (e) cycled DFM under 500 ppm NO₂-containing flue gas and EDX.



The nature and structure of carbon deposits on cycled Ni5Al15Ca DFMs were further examined by Raman spectroscopy, as shown in Fig. 12. The DFM cycled without SO₂ or NO₂ exhibited two prominent peaks centered at approximately 1357 cm⁻¹ (D band) and 1579 cm⁻¹ (G band), corresponding to amorphous carbon and graphitic sp² carbon, respectively. The intensity ratio (I_D/I_G) was used to evaluate the degree of graphitization. In the absence of SO₂ and NO₂, the cycled DFM displayed an I_D/I_G value of 1.1, indicative of the formation of highly graphitic carbon structures such as carbon nanotubes, consistent with TEM observations. Upon exposure to 100 ppm SO₂, the I_D/I_G ratio increased to 1.6, likely due to partial deactivation of Ni active sites. For DFMs exposed to 500 ppm SO₂, neither D nor G bands were detectable, indicating an absence of detectable carbon deposition, which was consistent with the TEM and reactor data. Introduction of NO₂ during the CO₂ capture stage showed minimal effect on the type of carbon formed during the CH₄ dry reforming step. However, carbon deposition was evidently suppressed, as corroborated by fixed-bed reactor results, even though the Raman spectra did not indicate significant changes in the graphitization degree.

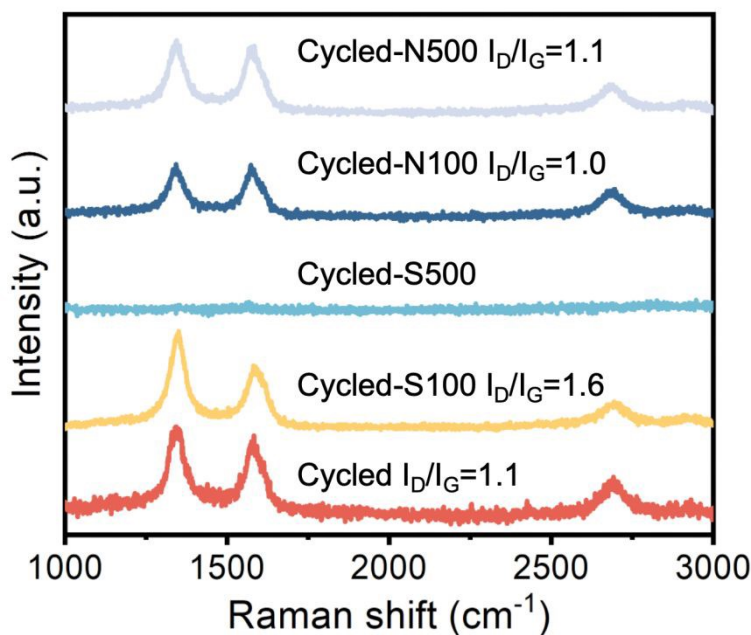


Fig. 12 Raman spectrum of cycled DFMs.

X-ray photoelectron spectroscopy (XPS) was conducted to gain insight into the surface elemental composition and chemical states of the cycled Ni5Al15Ca DFM, as shown in Fig. 13. Sulfur species were clearly detected on the surface after exposure to 100 ppm SO₂, with significantly intensified peaks under 500 ppm SO₂ conditions. Two characteristic S 2p signals at 163.2 eV and 172.4 eV were assigned to sulfide and sulfate species, respectively. Although only CaS was identified in the bulk phase by XRD, XPS analysis revealed that both sulfide and sulfate species were present on the surface in comparable proportions at lower SO₂ concentrations. Under 500 ppm SO₂, the surface was dominated by sulfide species, in agreement with the increased CaS content observed by XRD. In contrast, for the NO₂-treated DFM, no nitrogen species were detected on the surface after 10 cycles, suggesting that nitrogen-containing intermediates were fully decomposed or desorbed during the dry reforming process. This observation is consistent with both the elemental analysis and the absence of stable nitrogen-containing phases in the XRD results.



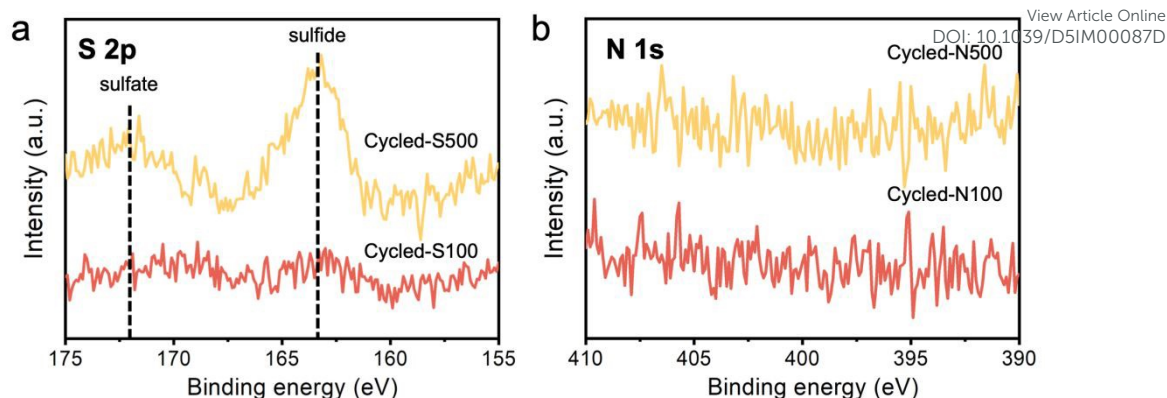


Fig. 13 XPS of cyclized DFM.

(a) SO₂-containing flue gas condition and (b) NO₂-containing flue gas condition.

Based on the above experimental findings, a mechanism is proposed to elucidate the influence of SO₂ and NO₂ on the ICCU-DRM process. During the CO₂ capture stage, both SO₂ and NO₂ can be co-adsorbed by CaO alongside CO₂. The generated CaS and CaSO₄ species are thermally stable and persist into the subsequent CH₄ dry reforming stage, whereas calcium nitrates formed from NO₂ adsorption are thermodynamically unstable and decompose upon gas switching. The formation of CaS and CaSO₄ can act as physical barriers that suppress CaO sintering and thereby enhance the cyclic stability of the DFM. However, progressive accumulation of these sulfur species leads to the irreversible consumption of active CaO, reducing the theoretical CO₂ uptake capacity. In the case of NO₂, the decomposition of calcium nitrates during cycling may contribute to improved pore structure, offering potential benefits for gas diffusion. During the CH₄ dry reforming stage, both SO₂ and NO₂ induce part or total deactivation of the Ni active sites through the formation of surface coating layers. NO₂ and low concentrations of SO₂ result in partial deactivation, leading to preserved CO₂ conversion but a notably reduced H₂:CO ratio and suppressed carbon deposition. In contrast, high SO₂ concentrations cause near-complete deactivation of Ni sites, eliminating both CO and H₂ production. This mechanistic insight highlights the nuanced and concentration-dependent effects of flue gas pollutants on ICCU performance, providing important guidance for the development of sulfur- and nitrogen-tolerant DFM materials in realistic industrial applications.

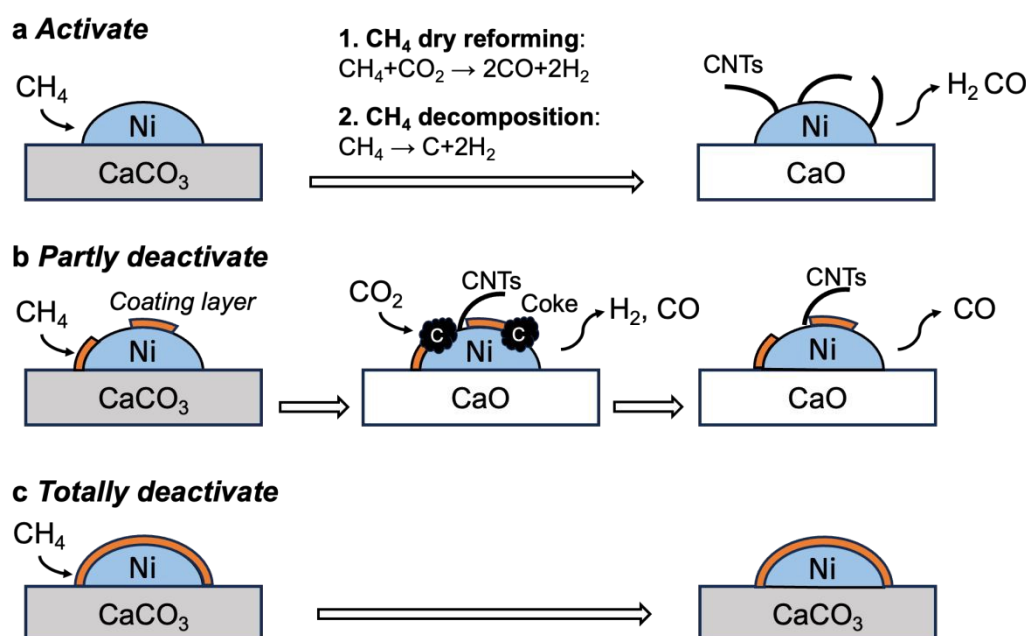


Fig. 14 Influence mechanism illustration of SO₂ or NO₂ pollutions in flue gas for ICCU-DRM.

3. Conclusions



In this study, we systematically evaluated the influence of SO₂ and NO₂ in flue gas to the ICCU-DRM performance and uncover relevant mechanism. Fixed-bed reactor results revealed that low concentration of SO₂ (100 ppm) in flue gas showed minor influence to the CO₂ conversion, but can effectively inhibit the methane decomposition side reactions, therefore significantly reduce the carbon deposition. Moreover, the low concentration of SO₂ in flue gas can effectively improve the stability of CO₂ capture. However, with the increase of SO₂ concentration to 500 ppm, the adsorption capacity and catalytic reforming capacity of the DFMs decreased significantly, and the materials were significantly deactivated after 10 cycles. NO₂ in flue gas exhibited similar trend with SO₂ but at lower impact level. Characteristics revealed that both SO₂ and NO₂ induced a coating layer on the surface of Ni catalytic site, which reduced the catalytic performance of the Ni active site, and then affect the performance of the DFM. This study provided a solid foundation for the design and application of DFMs under realistic flue gas conditions.

4. Experimental section

4.1 Material synthesis

The typical Ni5Al15Ca DFM was synthesized by a sol-gel method. Calculated amount of 15.11 g Ca(NO₃)₂·4H₂O (Aladdin, 99.9%), 4.50 g Al(NO₃)₃·9H₂O (Aladdin, 99.9%), and 1.16 g Ni(NO₃)₂·6H₂O (Aladdin, 99.9%) were dissolved in 60 mL deionized water and stirred for 1 h. 15.36 g citric acid (Aladdin, 99.5 %) was then added to the solution with another 1 h. Then the mixture was heated to 90°C with oil bath. The mixture formed a wet-gel after ca. 5 h, which was subsequently aged overnight in an oven at 120°C to form the dry-gel. The dry-gel was then calcined in a muffle furnace at 850°C for 2 h with a ramp rate of 10 °C min⁻¹. The as-synthesized powder was granulated to 40–60 mesh size. Finally, the Ni5Al15Ca DFM was pretreated in H₂ at 700°C for 3 h.

4.2 Material characterization

The molar ratios of Ni, Al, Ca and S in DFM were calculated using ICP-OES (Agilent ICPOES730) after digestion in nitric acid. The N element was analyzed by elementary analyzer (EA, Thermo Scientific Flash Smart Analyzer). Crystal structure of DFM was measured by XRD (PANalytical Empyrean series) equipped with a Bragg-Brentano high-definition mirror. The data was collected within the 2θ range of 10–90° with a step size of 0.01303° and 50 s per step. SEM (JEOL JSM-9700F) was applied to characterize the morphology and element distribution of the materials. Morphologies of nanoparticles and element distributions were investigated by TEM (JEOL JEM-2100 Plus, operated at 200 kV) equipped with EDX. The surface area and pore volume of the materials were determined by N₂ physisorption (Micromeritics, ASAP 2460 analyzer), with the Brunauer-Emmett-Teller (BET) model (using the adsorption data) and Barrett-Joyner-Halenda (BJH) model (using the desorption data), respectively. XPS (SPECS) with Al Kα X-ray source and PHOIBOS 150 Analyzer was performed for surface element analysis. The C 1s peak of adventitious carbon was set at 284.8 eV to correct for any charge-induced shifts. H₂-TPR (Micromeritics, AutoChem II-2920 system) was performed to evaluate the reducibility of the DFM. Ca. 100 mg sample was pretreated at 800 °C under Ar atmosphere. After cooling to room temperature, the sample was reduced at a ramp rate of 10°C min⁻¹ under 10% H₂/Ar from room temperature to 1000°C. The carbon capture capacity of DFM was evaluated by TGA (NETZSCH STA2500). Ca. 5 mg sample was placed in an alumina pan in the analyzer chamber and the weight signal was collected at 650°C under 15% CO₂/N₂.

4.3 Performance test of integrated carbon capture and methane dry reforming

The performance of integrated carbon capture and methane dry reforming (ICCU-DRM) was evaluated by a fixed-bed system. The gas analyzer (Cubic Ruiyi Instruments, Gasboard 3000) was used to analyzed the real-time concentration of gas. CO₂, CO and CH₄ was detected by non-dispersive infrared (NDIR) detector, while H₂ was detected by thermal conductivity detector (TCD). Briefly, ca. 200 mg DFM was placed in a quartz tube with an internal diameter of 8 mm. As for a typical ICCU-DRM test, the DFM was first pretreated under N₂ (50 mL min⁻¹) at 675°C to remove the adsorbed CO₂. Subsequently, the carbon capture stage was performed under 15%CO₂/N₂ (50 mL min⁻¹) at 650°C for 40 min. As for SO₂ and NO₂ containing flue gas, corresponding concentrations of SO₂ and NO₂ were mixed into the flue gas. The uncaptured CO₂ was purged by N₂ (50 mL min⁻¹) for 10 min. As for dry reforming stage, the DFM was exposed to 10% CH₄/N₂ (50 mL min⁻¹) at 675°C for 30 min, followed by purging by N₂ (50 mL min⁻¹) for 10 min. All working conditions repeated for 10 capture/conversion cycles to test the stability of the DFM. All experiments were operated at atmospheric pressure.

The CO yield in carbon capture stage, CO₂ uptake, CO₂ conversion, and H₂:CO ratio were calculated as below:

$$\text{CO yield in carbon capture stage (mmol g}^{-1}\text{)} = \frac{\int F_{\text{Cap,CO}}^{\text{out}}(t) dt}{m_{\text{DFM}}}$$

$$\text{CO}_2 \text{ uptake (mmol g}^{-1}\text{)} = \frac{\int [F_{\text{Cap,CO}_2}^{\text{in}}(t) - F_{\text{Cap,CO}_2}^{\text{out}}(t) - F_{\text{Cap,CO}}^{\text{out}}(t)/2] dt}{m_{\text{DFM}}}$$

$$\text{CO}_2 \text{ conversion (\%)} = \frac{\int F_{\text{Con,CO}}^{\text{out}}(t)/2 dt}{\int [F_{\text{Con,CO}}^{\text{out}}(t)/2 + F_{\text{Con,CO}_2}^{\text{out}}(t)] dt}$$



$$\text{H}_2:\text{CO ratio (1)} = \frac{\int F_{\text{Con,H}_2}^{\text{out}}(t) dt}{\int F_{\text{Con,CO}}^{\text{out}}(t) dt}$$

View Article Online
DOI: 10.1039/D5IM00087D

where, F denotes the molar flow rate of the gas, Cap and Con refers to carbon capture stage and conversion stage. M_{DFM} represents the mass of DFM.

4.4 In situ XRD

In situ XRD experiments were conducted on the XRD (PANalytical, Empyrean Series) equipped with an XRK 900 reactor chamber from Anton Paar (Anton Paar, XRK-900). The DFMs were firstly in situ reduced at 700°C under a flow of 100 mL min⁻¹ H₂ for 1 h, followed by purging in N₂. Subsequently, 100 mL min⁻¹ 2000 ppm SO₂/15% CO₂/N₂ was introduced into the chamber for 90 min. After another 100 mL min⁻¹ N₂ purge, 100 mL min⁻¹ 20% CH₄/N₂ was introduced into chamber for 90 min. The XRD patterns were continuously recorded with 2theta of 20–45° with 2.5 min per scan.

Author contributions

H.Z., S.S. and B.Y. conceived the research project. B.Y. designed the experimental work. B.Y., M.Y. and Y.W. performed the experiments. B.Y. contributed to the in situ XRD experiments. Y.X. and X.B. assisted with the catalyst characterization. Data analysis and interpretation were discussed among all coauthors. B.Y., S.S. and H.Z. wrote the manuscript, with contributions from all authors.

Conflicts of interest

There are no conflicts to declare.

Acknowledgements

This work was supported by the Beijing Natural Science Foundation (JQ24053), National Natural Science Foundation of China (52276202), National Key R&D Program of China (2023YFB4104000), Special support program for young talent innovation teams from Zhengzhou University (32320673), Carbon Neutrality and Energy System Transformation (CNEST) project (2023YFE0204600), International Joint Mission On Climate Change and Carbon Neutrality, and Tsinghua University Initiative Scientific Research Program.

References

- 1 J. Rogelj, M. Den Elzen, N. Höhne, T. Fransen, H. Fekete, H. Winkler, R. Schaeffer, F. Sha, K. Riahi and M. Meinshausen, Paris Agreement climate proposals need a boost to keep warming well below 2 °C, *Nature*, 2016, **534**, 631–639.
- 2 Z. Liu, Z. Deng, G. He, H. Wang, X. Zhang, J. Lin, Y. Qi and X. Liang, Challenges and opportunities for carbon neutrality in China, *Nat. Rev. Earth Environ.*, 2021, **3**, 141–155.
- 3 Z. Zhang, S.-Y. Pan, H. Li, J. Cai, A. G. Olabi, E. J. Anthony and V. Manovic, Recent advances in carbon dioxide utilization, *Renewable Sustainable Energy Rev.*, 2020, **125**, 109799.
- 4 D. U. Nielsen, X.-M. Hu, K. Daasbjerg and T. Skrydstrup, Chemically and electrochemically catalysed conversion of CO₂ to CO with follow-up utilization to value-added chemicals, *Nat. Catal.*, 2018, **1**, 244–254.
- 5 W. Gao, S. Liang, R. Wang, Q. Jiang, Y. Zhang, Q. Zheng, B. Xie, C. Y. Toe, X. Zhu, J. Wang, L. Huang, Y. Gao, Z. Wang, C. Jo, Q. Wang, L. Wang, Y. Liu, B. Louis, J. Scott, A.-C. Roger, R. Amal, H. He and S.-E. Park, Industrial carbon dioxide capture and utilization: State of the art and future challenges, *Chem. Soc. Rev.*, 2020, **49**, 8584–8686.
- 6 Y. Wang, R. Li, C. Zeng, W. Sun, H. Fan, Q. Ma and T.-S. Zhao, Recent research progress of methane dry reforming to syngas, *Fuel*, 2025, **398**, 135535.
- 7 A. H. K. Owgi, A. A. Jalil, I. Hussain, N. S. Hassan, H. U. Hambali, T. J. Siang and D. V. N. Vo, Catalytic systems for enhanced carbon dioxide reforming of methane: A review, *Environ. Chem. Lett.*, 2021, **19**, 2157–2183.
- 8 H. McLaughlin, A. A. Littlefield, M. Menefee, A. Kinzer, T. Hull, B. K. Sovacool, M. D. Bazilian, J. Kim and S. Griffiths, Carbon capture utilization and storage in review: Sociotechnical implications for a carbon reliant world, *Renew. Sust. Energ. Rev.*, 2023, **177**, 113215.



- 9 T. M. Gür, Carbon dioxide emissions, capture, storage and utilization: Review of materials, processes and technologies, *Prog. Energy Combust.*, 2022, **89**, 100965. View Article Online
DOI: 10.1039/D5IM00087D
- 10 J. Chen, Y. Xu, P. Liao, H. Wang and H. Zhou, Recent progress in integrated CO₂ capture and conversion process using dual function materials: A state-of-the-art review, *Carbon Capture Sci. Technol.*, 2022, **4**, 100052.
- 11 S. Sun, H. Sun, P. T. Williams and C. Wu, Recent advances in integrated CO₂ capture and utilization: A review, *Sustain. Energy. Fuels*, 2021, **5**, 4546–4559.
- 12 S. Sun, B. Yu, Y. Shen, Y. Liu, H. Sun, X. Bie, M. Wu, Y. Xu, C. Wu and H. Zhou, Promoting proximity to enhance Fe-Ca interaction for efficient integrated CO₂ capture and hydrogenation, *Sep. Purif. Technol.*, 2025, **357**, 130227.
- 13 E. García-Bordejé, J. M. Conesa, A. Guerrero-Ruiz and I. Rodríguez-Ramos, Bifunctional Na–Ru on gamma-alumina for CO₂ capture from air and conversion to CH₄: Impact of the regeneration method and support on monolithic contactors, *Ind. Chem. Mater.*, 2025, 10.1039.D5IM00030K.
- 14 H. Liu, L. Cen, X. Xie, L. Liu, Z. Sun and Z. Sun, Engineering nanoparticle structure at synergistic Ru-Na interface for integrated CO₂ capture and hydrogenation, *J. Energy Chem.*, 2025, **100**, 779–791.
- 15 Y. Shen, S. Sun, H. Sun, Y. Xu, H. Zhou, C. Wu and H. Qiu, Dual functional materials for integrated CO₂ capture and utilization (ICCU): Design, fabrication, performances, and challenges, *Chem. Eng. J.*, 2025, **512**, 162440.
- 16 Z. Lv, C. Qin, S. Chen, D. P. Hanak and C. Wu, Efficient-and-stable CH₄ reforming with integrated CO₂ capture and utilization using Li₄SiO₄ sorbent, *Sep. Purif. Technol.*, 2021, **277**, 119476.
- 17 B. Shao, G. Hu, K. A. M. Alkebsi, G. Ye, X. Lin, W. Du, J. Hu, M. Wang, H. Liu and F. Qian, Heterojunction-redox catalysts of Fe_xCo_yMg₁₀CaO for high-temperature CO₂ capture and in situ conversion in the context of green manufacturing, *Energy Environ. Sci.*, 2021, **14**, 2291–2301.
- 18 S. Bahrami Gharamaleki, S. Carrasco Ruiz, T. Ramirez Reina, M. Short and M. S. Duyar, Effect of adsorbent loading on NaNiRu-DFMs' CO₂ capture and methanation: Finding optimal Na-loading using Bayesian optimisation guided experiments, *Ind. Chem. Mater.*, 2025, 10.1039.D5IM00019J.
- 19 S. Sun, Y. Wang, Y. Xu, H. Sun, X. Zhao, Y. Zhang, X. Yang, X. Bie, M. Wu, C. Zhang, Y. Zhu, Y. Xu, H. Zhou and C. Wu, Ni-functionalized Ca@Si yolk-shell nanoreactors for enhanced integrated CO₂ capture and dry reforming of methane via confined catalysis, *Appl. Catal., B*, 2024, **348**, 123838.
- 20 J. Hu, P. Hongmanorom, V. V. Galvita, Z. Li and S. Kawi, Bifunctional Ni-Ca based material for integrated CO₂ capture and conversion via calcium-looping dry reforming, *Appl. Catal., B*, 2021, **284**, 119734.
- 21 Y. Hu, H. Lu, W. Liu, Y. Yang and H. Li, Incorporation of CaO into inert supports for enhanced CO₂ capture: A review, *Chem. Eng. J.*, 2020, **396**, 125253.
- 22 H. Sun, C. Wu, B. Shen, X. Zhang, Y. Zhang and J. Huang, Progress in the development and application of CaO-based adsorbents for CO₂ capture—A review, *Mater. Today Sustain.*, 2018, **1–2**, 1–27.
- 23 Y. Hu, Q. Xu, X. Zou, X. Wang, H. Cheng, X. Zou and X. Lu, M_xO_y (M = Mg, Zr, La, Ce) modified Ni/CaO dual functional materials for combined CO₂ capture and hydrogenation, *Int. J. Hydrog. Energy*, 2023, **48**, 24871–24883.
- 24 Y. Guo, G. Wang, J. Yu, P. Huang, J. Sun, R. Wang, T. Wang and C. Zhao, Tailoring the performance of Ni-CaO dual function materials for integrated CO₂ capture and conversion by doping transition metal oxides, *Sep. Purif. Technol.*, 2023, **305**, 122455.
- 25 X. Xu, B. Yu, M. S. Hussain, Y. Wang, Q. Li, Y. Xu, Y. Zhang and H. Zhou, One-pot synthesis of cost-effective dual functional material from solid waste for integrated CO₂ capture and utilization, *Sep. Purif. Technol.*, 2025, **372**, 133309.
- 26 N. Pegios, G. Schroer, K. Rahimi, R. Palkovits and K. Simeonov, Design of modular Ni-foam based catalysts for dry reforming of methane, *Catal. Sci. Technol.*, 2016, **6**, 6372–6380.



- 27 E. Wang, Z. Zhu, R. Li, J. Wu, K. Ma and J. Zhang, Ni/CaO-based dual-functional materials for calcium-looping CO₂ capture and dry reforming of methane: Progress and challenges, *Chem. Eng. J.*, 2024, **482**, 148476. View Article Online
DOI: 10.1039/D5IM00087D
- 28 S. Jo and K. L. Gilliard-AbdulAziz, Self-regenerative Ni-doped CaTiO₃/CaO for integrated CO₂ capture and dry reforming of methane, *Small*, 2024, 2401156.
- 29 Y. Zhao, R. Hao, T. Wang and C. Yang, Follow-up research for integrative process of pre-oxidation and post-absorption cleaning flue gas: Absorption of NO₂, NO and SO₂, *Chem. Eng. J.*, 2015, **273**, 55–65.
- 30 X. Zhou, H. Yi, X. Tang, H. Deng and H. Liu, Thermodynamics for the adsorption of SO₂, NO and CO₂ from flue gas on activated carbon fiber, *Chem. Eng. J.*, 2012, **200–202**, 399–404.
- 31 R. Chen, T. Zhang, Y. Guo, J. Wang, J. Wei and Q. Yu, Recent advances in simultaneous removal of SO₂ and NO_x from exhaust gases: Removal process, mechanism and kinetics, *Chem. Eng. J.*, 2021, **420**, 127588.
- 32 A. Bhaskaran and S. Roy, Exploring dry reforming of CH₄ to syngas using high - entropy materials: A novel emerging approach, *ChemCatChem*, 2025, **17**, e202401297.
- 33 T. Y. Yeo, J. Ashok and S. Kawi, Recent developments in sulphur-resilient catalytic systems for syngas production, *Renew. Sust. Energ. Rev.*, 2019, **100**, 52–70.
- 34 H. Li, X. Peng, M. An, J. Zhang, Y. Cao and W. Liu, Negative effect of SO₂ on mercury removal over catalyst/sorbent from coal-fired flue gas and its coping strategies: A review, *Chem. Eng. J.*, 2023, **455**, 140751.
- 35 H. Yu, C. Shan, J. Li, X. Hou and L. Yang, Alkaline absorbents for SO₂ and SO₃ removal: A comprehensive review, *J. Environ. Manage.*, 2024, **366**, 121532.
- 36 N. Ding, Y. Zheng, C. Luo, Q. Wu, P. Fu and C. Zheng, Development and performance of binder-supported CaSO₄ oxygen carriers for chemical looping combustion, *Chem. Eng. J.*, 2011, **171**, 1018–1026.



Data availability statement

The data that support the findings of this study are available from the corresponding author upon reasonable request.

